American Mineralogist, Volume 98, pages 609–615, 2013

Noise of collapsing minerals: Predictability of the compressional failure in goethite mines

Ekhard K.H. Salje,[1,*] Giulio I. Lampronti,[1] Daniel E. Soto-Parra,[2] Jordi Baró,[3] Antoni Planes,[3] and Eduard Vives[3]

[1]Department of Earth Sciences, University of Cambridge, Downing Street, Cambridge CB2 3EQ, U.K.
[2]Instituto Potosino de Investigación Científica y Tecnológica, División de Materiales Avanzados, Camino a la Presa San José 2055, Col. Lomas 4a. sección C.P. 78216, San Luis Potosí, México
[3]Department Estructura i Constituents de la Matèria, Facultat de Física, Universitat de Barcelona, Martí i Franquès 1, 08028 Barcelona

Abstract

Compression experiments of goethite samples from an iron ore mine in New Caledonia revealed the collapse of the porous samples to follow a power law behavior. The porosity varies between 54 and 84%. The collapse under compression occurs in a series of individual events (avalanches). Each avalanche leads to a jerk in sample compression and an equivalent acoustic emission signal. The probability to find an acoustic emission signal with an energy within E and $E + dE$ is $p(E)dE$, which has a power law distribution $p(E) \sim E^{-\varepsilon}$, and reveals avalanche criticality. The energy exponent ε varies systematically with the porosity of the sample between 1.6 and 2. The results are compared with previous measurements of porous silica (Vycor), which showed a slightly smaller exponent of 1.4.

We observe fore- and after-shocks of the largest events. Significant correlations between the largest avalanches and fore-shocks were found in samples with high porosity. These correlations open the possibility for the prediction of a major collapse by acoustic detection of noise.

Keywords: Goethite, porous materials, stress failure, crackling noise, power law collapse

Introduction

The structural stability of minerals and mineral assemblies is a key ingredient for the safety of mines, the durability of building stones and the use of minerals in medical applications. Mining involves very often porous mineral assemblies (Hudson-Edward et al. 1999; Traore et al. 2008), including goethite, pyrite, and coal, which lead to serious accidents when landslides occur in open mining or when mining shaft collapse. Such catastrophic events are sometimes announced by acoustic precursors of the collapse (Bai et al. 1994; Tornos 2006). Most historic building stones are porous and damage is affected when they are mechanically sheared or compressed (Rodriguez-Navarro et al. 1996; Benavente et al. 2004), and many rocks such as shales and volcanic extrusions also display high porosity, which is important for their use in, say, CO_2 sequestration or as host rock for oil and other liquids (Gurevich 1995; Alatorre-Ibarguengoitia et al. 2011; Kawada et al. 2010; Rathore et al. 1995; Spieler et al. 2004; Jakobsen et al. 2000). Other applications of porous materials relate to medical implementations such as titanium foams and ceramic hip replacements. Here the failure mechanism is crucial for choice of the proper implant material (Kashef et al. 2011; Boden et al. 2008). The typical failure under shear stress is that porous material "snaps" when exposed to the critical shear stress. Crack propagation is fast and few intermediate states were observed at low temperatures. Snapping becomes more viscous for torsion pendulum experiments at high temperatures near the melting point where grain boundary sliding and dislocation creep become dominant (e.g., Vallely and Gillham 1997; Jackson and Faul 2010).

Uniaxial compression leads to a completely different picture, however. The collapse of the sample is gradual and progresses by avalanches, which can be detected by Acoustic Emission (AE) experiments. In a recent study, Salje et al. (2011) used a porous glass material (Vycor) to show that these avalanches follow almost perfect power law statistics ("crackling noise") with a characteristic critical exponents similar to those measured in mechanical instabilities in martensites and ferroelastic materials (Salje et al. 2009a, 2009b; Carrillo et al. 1998; Bonnot et al. 2008), critical dynamics in microfracturing (Petri et al. 1994), and spontaneous AE in volcanic rocks (Diodati et al. 1991). This has put the problem of understanding the failure of porous materials under compression within the scenario of crackling noise and avalanche criticality.

While several models for the failure criteria under compression have been discussed (e.g., Deshpande et al. 2001; Girard et al. 2012) most "conventional" porous minerals show only two characteristics to dominate the collapse. The first relates to the moduli of the mineral skeleton, which can be derived from the bulk material. The second key feature is the porosity of the mineral assembly. A universal theory for the stability of dry and porous minerals and mineral assemblies is known not to exist. The reasons are that the stability point also depends on the on the topology of the mesoscopic structure. Furthermore, the stability criteria vary on the length scale over, which the sample is considered (see Michel et al. 2007, for a review). What is possible, however, is to formulate such rules when the porous microstructure is fully known on a mesoscopic scale. This attempt has been made for voids in the shape of spheres or ellipsoids and defined degrees of cross-linking of the framework (Boker et al. 2007). Several investigations have been dedicated

* E-mail: ekhard@esc.cam.ac.uk

0003-004X/13/0004–609$05.00/DOI: http://dx.doi.org/10.2138/am.2013.4319

to the evaluation of elastic moduli for given microstructures starting with Hill (1972) and Scherer (1998). Similarly, the calculations for the onset of failure, e.g., under a load parameter such as a shear stress in a randomly oriented mineral assembly, leads to several failure mechanisms. Local failures include the percolation of voids, instabilities related to the free surfaces of the voids, "strain lock up" (Michel et al. 2007) with large strains at the inner surfaces of the pores, and pore closure, which also leads to a sudden collapse of the sample (Muralidharan and Hui 2004). The situation becomes greatly simplified if we consider "conventional" porous minerals, which do not contain highly anisotropic grains (fibers and platelets) and where the effective bulk modulus κ is approximated by

$\kappa/\kappa_m = 1 - \Phi/\Phi_c$ with $\Phi_c \approx 0.5$ for low porosity and

$\kappa/\kappa_m \sim (1 - \Phi)^m$ with $m \approx 3.2$ for high porosity,

where Φ and κ_m are the porosity and the matrix modulus, respectively. The failure occurs at a strength of some 10^{-3} κ, which leads to typical instabilities at porosities near 0.8–0.9 for gravity forces of some 100 kPa (Salje et al. 2010; Traore et al. 2008). An 80% porosity is indeed experimentally observed as a maximum porosity in freely drained regoliths and similar mining circumstances.

To prevent mining accidents it is desired to have some "early warning system" before the main collapse happens. The simplest idea is that the collapse is accompanied by precursor shocks and, most importantly for rescue operations, by aftershocks.

In this paper, we describe the collapse of mineral assemblies from a goethite mine in New Caledonia. AE is detected during compression experiments to show that for highly porous mineral assemblies (>50% porosity) noise does increase just before the major collapse but that such precursor effects do not exist for assemblies with low porosity. Results are compared with those reported for an artificially grown Vycor porous material.

The AE technique: General features

Changes in the internal strain field of a solid associated with moving dislocations (Rouby et al. 1983a, 1983b), rapid structural transformations (Mañosaet al. 1989) or crack propagation (Petri et al. 1994) are accompanied by the emission of acoustic waves. This AE carries information on the source mechanism, and thus, its detection is potentially useful for the investigation of externally stimulated processes, which occur in solids at scales ranging from nano- to micrometers. From a technological point of view detection of AE provides a powerful nondestructive testing technique, which enables monitoring of damage processes during their entire history without any disturbance of the analyzed specimen.

Detection of AE signals is commonly performed using a piezoelectric transducer coupled directly to the studied specimen or by means of a waveguide. To study the statistical features of AE signals characterizing the avalanches occurring during the compression process, resonant transducers characterized by a relatively narrow operation range between 200 kHz and 2 MHz and typically centered about 1 MHz are adequate due to their high sensitivity to very small (down to tens of nanometers) displacement discontinuities. The transducer produces a voltage, which is amplified and filtered to suppress low- and high-frequency noise. This voltage $U(t)$ is then digitized and finally stored for further processing. Processing first requires the identification of individual events, which is followed by the extraction of the required information. For the identification of events a threshold set above the remaining background noise is used. A hit is commonly assumed to start with the first crossing of the threshold at an initial time t_0. The duration of an event is given by $\Delta t = t_f - t_0$, where the end time t_f is the time at which the signal voltage falls below the threshold for more than a preset hit detection time (typically fixed between 10 and 100 μs). The energy associated with the event is computed as

$$E = \frac{1}{R}\int_{t_0}^{t_f} U^2(t)\,dt \quad (1)$$

where R is a reference electrical resistance. AE activity is usually defined as the number of hits detected during a given time interval. This time interval is chosen to be of about 1 s and therefore this quantity represents an integrated measurement on a long timescale.

The AE signals provide information regarding size and duration of the avalanches occurring during the studied dynamical process thus reflecting its collective behavior. When analyzing experiments, it is often observed that the energy of the AE signals spans over several orders of magnitude. Many small signals are detected, and fewer and fewer signals of a larger and larger energy are recorded. The distribution of amplitudes, energies, and duration often follow a power law within the measurement window to a good approximation. This is indicative of the fact that the process evolves with the absence of characteristic scales, which is a typical feature of criticality. This kind of criticality is related to the properties of the avalanches (avalanche criticality) (Sethna et al. 2006). Thus the dynamics show scale invariance, which means that the same distribution of avalanche energies must occur when the scale of observation is changed.

Sample characterization

Samples of brown goethite ore were extracted from the ultramafic Koniambo outcrops (20°59′ S; 164°49′ E) located in the northern province of the Grande Terre, on the western coast of New Caledonia. These samples were described already by Schwertmann and Latham in 1985 and were analyzed mineralogically by Fandeur et al. (2009). They were provided by E. Fritsch (Université Paris VI) (Fritsch et al. 2007). The geological setting is related to the obduction of ultramafic rocks (mainly peridotites) at the Upper Eocene (38 Ma) and is characterized by a complex geological setting essentially made of harzburgite, with gabbro and dunite intrusions. These mafic and ultramafic rocks are affected by a network of large fractures related to hydrothermal fluids generated during the obduction event. Deep weathering of these ultramafic rocks under tropical conditions led to the development of a lateritic regolith defined by the succession of a peridotite bedrock unit, a saprolite unit and a laterite unit, from the bottom to the surface.

Tables 1a and 1b show the mineralogical composition, the depth of the location of the samples, and their porosity. For each sample a parallelepiped-shaped specimen was cut and its volume

Table 1a. Mineralogical composition (in wt%) of the analyzed samples as obtained from the Rietveld refinements and relative goodness of fit; the e.s.d. relate to the mathematical fit and do not represent error in precision or accuracy

Sample	Goethite	Magnetite	Clinochrys.	Orthopyroxene	GOF
YL25m	88.1%±3.8%	<5%	7.1 ± 1.4%	not included	1.342
BW39m	78.2%±1.4%	<5%	16.0 ± 1.2%	not included	1.185
YL8m	92.3%±1.1%	<5%	<5%	not included	1.410
BW39m(second)	62.3%±1.0%	<5%	25,3 ± 1.0%	not included	1.198
HZ54.8m	63.6%±1.9%	5.2 ± 0.4%	16.1 ± 1.3%	11.1 ± 0.8%	1.257
YL17m	96.2%±9.9%	<5%	<5%	not included	1.362

Table 1b. Porosity and amorphous fraction (in wt%) of each sample

Sample	Depth of the extraction	Porosity	Amorphous fraction
BW39m	39 m	Φ = 0.83	58.1%
BW39m(second)	39 m	Φ = 0.84	55.7%
YL25m	25 m	Φ = 0.82	53.7%
HZ54.8m	54.8 m	Φ = 0.80	34.6%
YL17m	17 m	Φ = 0.65	54.4%
YL8m	8 m	Φ = 0.54	56.1%

Note: Talc, quartz, and taramite fractions are not reported as they were found to be always smaller than 5 wt%.

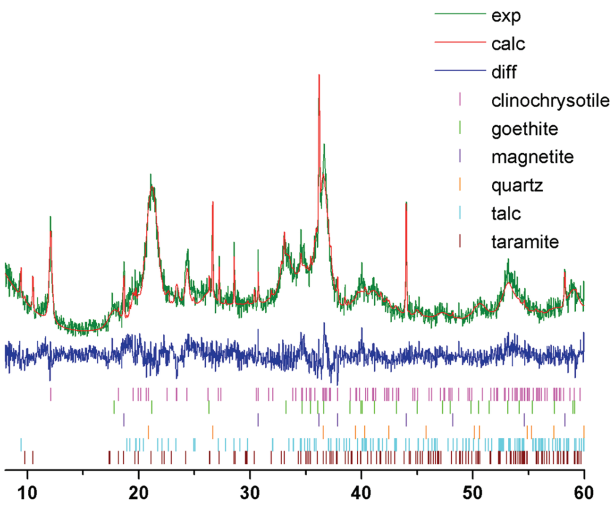

Figure 1. Experimental, calculated, and difference patterns for sample BW39m(second); the x-axis is in degrees of 2θ. Peak positions for all the present phases are marked with different colors. (Color online.)

measured; the specimen was then pelletized under a pressure of about 10 tons/cm^2 for 1 min, and its volume measured again to estimate the sample porosity. The samples were slightly heterogeneous but repeated runs using several specimens cut from the same sample gave similar results. We will use the term "goethite" in this paper to indicate these samples.

X-ray powder diffraction diffractograms in the 2θ range of 5–60° (step size, 0.03°; time/step, 30 s; VxA, 40 × 40) were collected on a D8 Bruker diffractometer equipped with a primary Ge monochromator for Cu$K\alpha_1$ and a Sol-X solid-state detector. Rietveld refinements were performed with the software TOPAS 4.1 (Cohelo 2007). Crystal structures of all phases were retrieved from either the Crystallographic Open Database (Grazulis et al. 2009) or from the Inorganic Cambridge Structural Database (Allmann et al. 2007): goethite (Hazemann et al. 1991); magnetite (Bragg 1915); clinochrysotile (Whittaker 1956); talc (Rayner and Brown 1973); quartz (Levien et al. 1980); taramite (Oberti et al. 2007); orthopyroxene (Chatterjee et al. 2009).

The March-Dollase model for preferred orientation (Dollase 1986) was applied on the following crystal planes: (1 1 0) and (1 1 1) for goethite; (1 0 0) and (1 1 1) for magnetite; (1 0 0) for clinochrysotile; (0 0 1) for talc; (1 0 1) for quartz; (0 1 0) and (1 2 0) for taramite; (2 1 0) and (6 1 0) for orthopyroxene. No structural parameter was refined. A shifted Chebyshev function with 10 parameters was used to fit the background. Peak shapes of all phases were modeled using pseudo-Voigt functions. Figure 1 shows experimental, calculated, and difference curves for sample BW39m (second). Table 1 reports weighted percentages of phases and physical details for all samples; the reported e.s.d. have no bearing on the accuracy or otherwise of the quantification itself, being merely related to the mathematical fit of the model (Madsen and Scarlett 2008). Rietveld quantitative analysis is known to be unreliable in the presence of phases with strong preferred orientation such as talc and chrysotile. Thus, the Rietveld refinements were repeated with and without correction for preferred orientations for some or for all phases as a test: while the goethite fractions changes by no more than 10% of the reported values, the quantification trends are preserved, so that YL17m as an example is always the sample with the largest content of goethite.

The amorphous content of the samples was estimated with the internal standard method (Madsen and Scarlett 2008). A specimen of each sample was mixed with 15 wt% of corundum, which was used as an internal standard. Powder diffraction data were collected and analyzed again. The amorphous content was estimated to be 54 to 58 wt%. The only exception is sample HZ54.8m in which the amorphous content was found to be 34.6 wt%.

To understand the chemical nature of the amorphous matrix, samples YL25m, YL8m, BW39m, and BW39m(second) were embedded in epoxy resin to perform electron microprobe chemical analysis. Unfortunately the totals for each analysis were far below 90%, likely due to the high porosity of the samples. The resin infilling the pores affected the analysis to no measurable degree. Qualitatively, however, the analysis illustrated that samples BW39m and BW39m(second) contain a higher weight percentage of silica and alumina than YL25m and YL8m.

Experimental methods

Slow compression tests were performed on nine mesoporous "goethite" specimens, which were taken from the six original samples. Prismatic specimens were cut with a knife to cubes with dimensions of 5 × 5 × 5 mm approximately. When possible, the surfaces were polished to a flat plane with sandpaper. The specimens were tested at constant stress rates of 0.005 N/s (±0.01 N/s).

Specimens are placed between two aluminum plates as shown in Figure 2. The lower plate is attached to the load cell hanging from the ceiling. The compression force is applied by supplying water at a constant rate to a container hanging from the upper plate, which can move vertically through three linear bearings that act as guides. This method allows a control of the stress rate applied to the sample.

The average shrinkage of the sample was estimated by measuring the separation between the two plates using a laser extensometer with a nominal resolution of 0.1 μm. Two piezoelectric transducers (micro-80) were embedded to the upper and lower plates and act as a wave-guide with the aim to increase the number of independently detected signals, since samples exhibit high-acoustic attenuation. The electric signals from the transducers were pre-amplified (60 dB) and input to a PCI2 acquisition system from Euro Physical Acoustic SA working at 1MSPS (1 MHz). This system determines the energies of the AE events, which are obtained

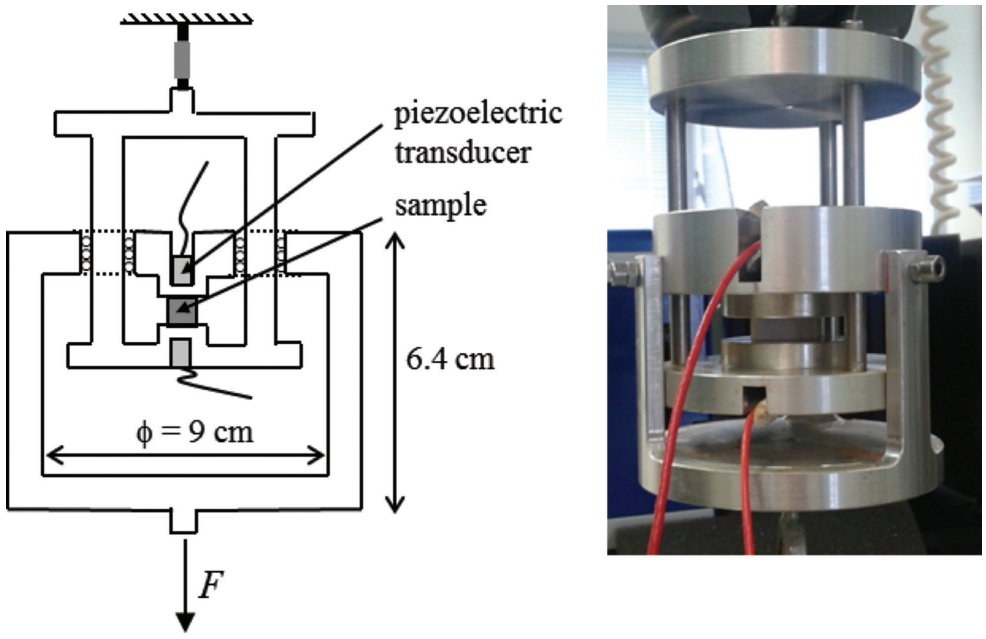

FIGURE 2. Schematic representation and photograph of the compression arrangement. (Color online.)

by fast integration of the square voltage of signals detected above a given threshold (26 dB) as previously explained. The AE activity (counts/s) was computed as the number of AE events recorded by the two sensors in an interval of 20 s.

RESULTS

Examples of acoustic emission activities are shown in Figure 3 and 4. For both samples the length X of the sample itself, the squared time derivative $(dX/dt)^2$ and the acoustic activity (counts/s) are shown. The correlation between the acoustic activity and $(dX/dt)^2$ is evident. This is in agreement with the hypothesis that AE is proportional to the dissipated energy during the failure process.

In all cases a sudden collapse is seen in the length $X(t)$, which leads to large time derivatives and high-acoustic emissions. The acoustic activity is not restricted to the time interval of the collapse but occurs over the whole time span of the experiment. Even at times after the collapse, the debris contains still porous but intact regions, which collapse when stress is increased further.

In the log-log plot in Figure 5, we show the energy distribution $p(E)$ of jerks [a "jerk" is defined as a spike in a noise spectrum; here we have such jerks in the squared time derivative of the length $(dX/dt)^2$ or as acoustic emission signals] as function of the energy E. We have included in this figure the previous results for Vycor (Salje et al. 2011). Different experiments corresponding to specimens cut from the same sample are plotted with the same symbol shapes.

As can be seen the histograms are quite linear in this plot. This suggests that the distribution of energies is a power law

$$p(E)dE = \frac{E^{-\varepsilon}}{E_{\min}^{1-\varepsilon}}dE \qquad E_{\min} < E < \infty ,$$

where $E_{\min}$ is a lower cutoff needed for normalization. The lines in Figure 5 are guides to the eye. They already reveal the increasing

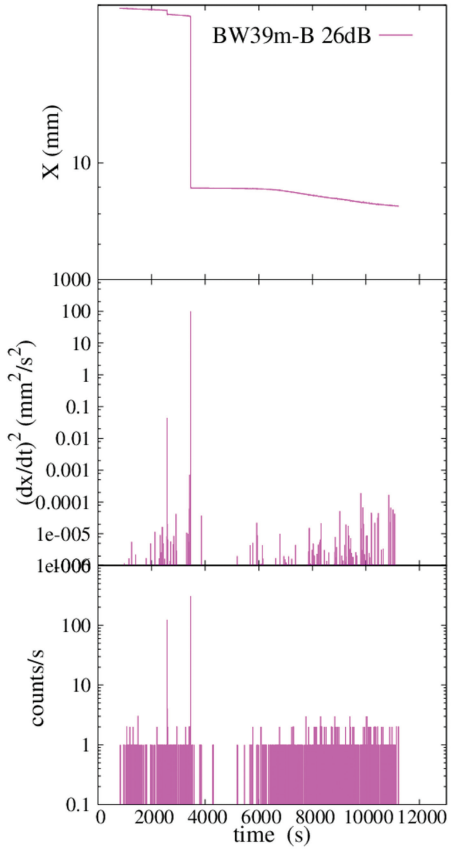

FIGURE 3. Example of AE and extensometer data recorded during the compression experiment of a sample with high porosity. The vertical scales in the two lower plots are logarithmic. (Color online.)

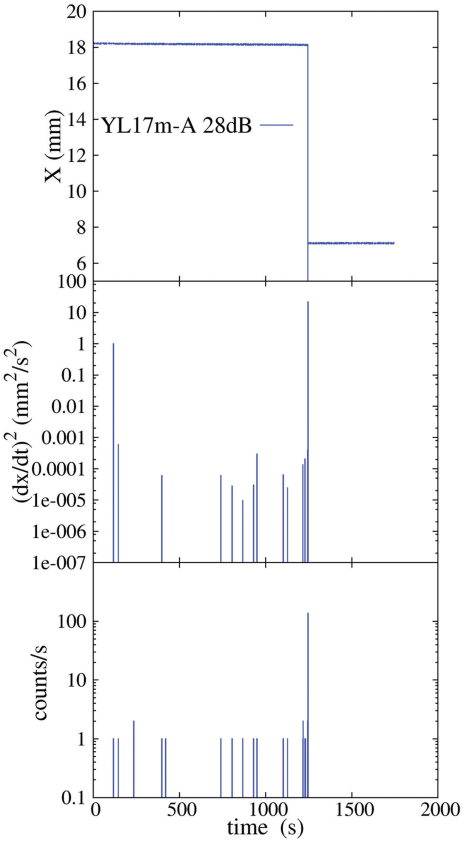

FIGURE 4. Example of AE and extensometer data recorded during a compression experiment of a low porosity speciment. The vertical scales in the two lower plots are logarithmic. (Color online.)

value of the exponent ε with porosity.

Quantitative power-law exponents can be obtained using the maximum likelihood method. Here we applied the treatment proposed by (Baró and Vives 2012). The exponent is fitted by considering a higher cutoff equal to the maximum energy measured, while the lower cutoff varies within several orders of magnitude. It is expected (Baró and Vives 2012; Clauset et al. 2009) that the fitted exponent should exhibit a plateau for several orders of magnitude. Indeed this was the case in the previous studies with Vycor, while in the case of goethite the plateau is not as clean most likely because the statistics are much poorer. Figure 6 shows selected examples.

DISCUSSION

The acoustic activity spectra can be divided into two groups. High-porosity samples activity show a similar behavior over large time intervals, and reveal two extra features near the major collapse of the sample itself. In the pre-collapse stage, we find an interval of ca. 1000 s before the major event where acoustic activity is enhanced beyond the statistical expectation value. This corresponds to the desired precursor effect, which could be used as early warning signal. The effect is seen in all samples with high porosity and can be extreme, although in some cases this acoustic signal is less intense. In samples with low porosity, no such precursor effect exists and acoustic emission remains

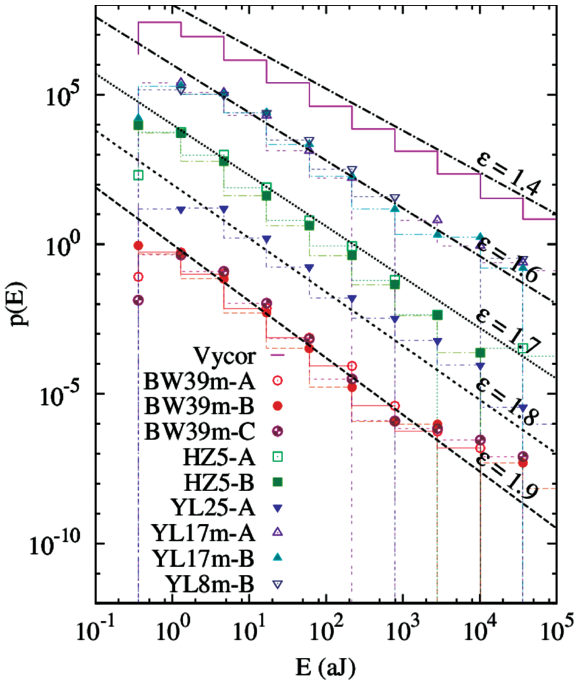

FIGURE 5. Histograms corresponding to the energy distribution of the AE events for the different experiments in this work. We also show, for comparison, the histogram corresponding to previous experiments with Vycor (Salje et al. 2011). The lines are guides to the eye that illustrate selected values of the power-law exponent. (Color online.)

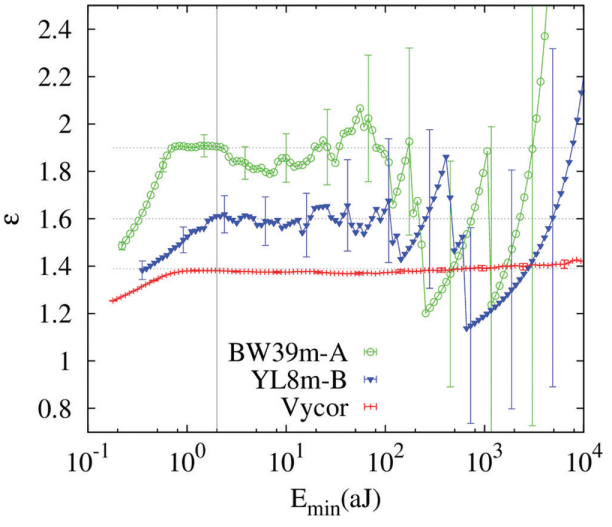

FIGURE 6. Maximum likelihood power-law exponent as a function of the minimum cutoff E_{min} for two goethite experiments, compared to the behavior of a synthetic porous material Vycor. (Color online.)

statistically constant and independent of the major collapse.

The second observation concerns the gap in some samples after the major event, i.e., a time interval of around 1000 s where the acoustic activity is reduced for the highly porous samples. Less porous sample (e.g., Fig. 3) do not show such reduction.

Interestingly the Vycor sample with a porosity of 0.4 (i.e., less porous in the context of this study) shows features similar to those of the least porous goethite samples: a similar noise

spectrum with no detectable noise gap after the major collapse. The major difference between goethite and Vycor is seen in Figures 5 and 6: the Vycor sample shows a power-law distribution of the acoustic emission spectra over a very large interval of six orders of magnitude. In contrast, the power law approximation is found to hold in goethite only for three orders of magnitude while deviations occur for higher energy events. Furthermore, the power-law exponents for goethite are larger than the value of 1.39 of the Vycor sample.

Figure 7 shows that there is a clear dependence between the exponent ε and the porosity Φ. This indicates that at high-porosity failures are characterized by a large proportion of small jerks relative to the large events, while low porosity minerals fail with a relatively lower fraction of small events. The time distribution of the events shows that precursor and after-shock events are correlated with big events in case of high-porosity samples. The same is not true for samples with lower porosity. This scenario makes it virtually impossible to predict the main collapse from the observation of precursor noise for samples with porosities lower than some 80%.

Concluding remarks

In the present paper, we studied the acoustic behavior of natural mesoporous goethite ore samples with porosity of 54 to 84% during uniaxial compression loading. Acoustic signals are observed before and after the main collapse events. The probability distribution of acoustic emission signals and related energies within E and $E+dE$ is a power law, $p(E) \sim E^{-\varepsilon}$, and shows scale invariance, therefore. The origin of the power law is the avalanche propagation of the collapse. We found a significant correlation between the largest avalanches and the correspondent foreshocks in the case of high porosity (>80%). These experimental observations lead to the possibility of large-scale major collapses prediction by the detection of acoustic signals in the case of geological materials constituted by crystalline (or amorphous) bulk phases with a highly porous microstructure, such as goethite, pyrite, and coal mines rocks. Moreover acoustic signal analysis can be applied in research fields that involve any highly porous material; we are currently working on the acoustic behavior of aluminum oxide porous ceramics. On the other hand in case of samples with lower porosity, no such correlations were found and avalanche predictions become virtually impossible.

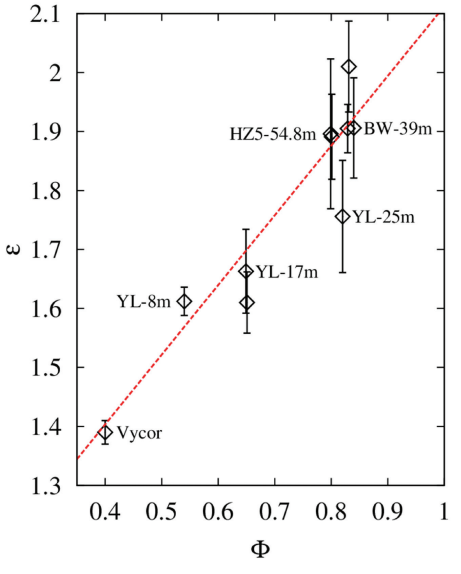

Figure 7. Power-law exponent ε as a function of the porosity Φ for the different goethite specimens studied in this work and for the Vycor sample (Salje et al. 2011). (Color online.)

Acknowledgments

We thank Iris Buisman (Department of Earth Sciences, University of Cambridge) for her help on the electron microprobe. This work has been partially funded by CICyT (Spain) through project MAT2010-15114. E.K.H.S. is grateful to the Leverhulme foundation for financial support (RPG-2012-564).

We are grateful to Emanuel Fritsch for providing the samples (IPGP Paris) and to S. Gorfman (Univ. Siegen) for helpful discussions.

References cited

Alatorre-Ibarguengoitia, M.A., Scheu, B., and Dingwell, D.B. (2011) Influence of the fragmentation process on the dynamics of Vulcanian eruptions: An experimental approach. Earth and Planetary Science Letters, 302, 51–59.

Allmann, R. and Hinek, R. (2007) The introduction of structure types into the Inorganic Crystal Structure Database ICSD. Acta Crystallographica, A63, 412–417.

Bai, M. and Elsworth, D. (1994) Modelling of subsidence and stress-dependent hydraulic conductivity for intact and fractured porous-media. Rock Mechanics and Rock Engineering, 27, 209–234.

Baró, J. and Vives, E. (2012) Analysis of power-law exponents by maximum-likelihood maps. Physical Review E, 85, 066121.

Benavente, D., del Cura, M.A.G., Fort, R., and Ordonez, S. (2004) Durability estimation of porous building stones from pore structure and strength. Engineering Geology, 74, 113–127.

Boden, B.P. and Jarvis, C.G. (2008) Spinal injuries in sports. Neurologic Clinics, 26, 63–78.

Boker, A., He, J., Emrick, T., and Russell, T.P. (2007) Self-assembly of nanoparticles at interfaces. Soft Matter, 3, 1231–1248.

Bonnot, E., Mañosa, L., Planes, A.,Soto-Parra, D., Vives, E., Ludwig, B., Strothkaemper, C., Fukuda, T., and Kakeshita, T. (2008) Acoustic emission in the fcc-fct martensitic transition of Fe(68.8)Pd(31.2). Physical Review B, 78, 184103.

Bragg, W.H. (1915) The structure of magnetite and the spinels. Nature, 95, 561.

Carrillo, L., Mañosa, L., Ortin, J., Planes, A., and Vives, E. (1998) Experimental evidence for universality of acoustic emission avalanche distributions during structural transitions. Physical Review Letters, 81, 1889–1892.

Chatterjee, S., Sengupta, S., Saha-Dasgupta, T., Chatterjee, K., and Mandal, N. (2009) Site preference of Fe atoms in $FeMgSiO_4$ and $FeMg(SiO_3)_2$ studied by density functional calculations. Physical Review B, 79, 115103.

Clauset A., Shalizi C.R., and Newman, M.E.J. (2009) Power-law distributions in empirical data. SIAM Review, 51, 661–703.

Cohelo, A. (2007) TOPAS-Academic, Coelho Software, Brisbane, Australia.

Deshpande, V.S., Fleck, N.A., and Ashby, M.F. (2001) Effective properties of the octet-truss lattice material. Journal of the Mechanics and Physics of Solids, 49, 1747–1769.

Diodati, P., Marchesoni, F., and Piazza, S. (1991) Acoustic emission from volcanic-rocks and example of self-organized criticality. Physical Review Letters, 67, 2239–2243.

Dollase, W.A. (1986) Correction of intensities for preferred orientation in powder diffractometry: application of the March model. Journal of Applied Crystallography, 19, 267–272.

Fandeur, D., Juillot, F., Morin, G., Olivi, L., Cognigni, A., Webb, S.M., Ambrosi, J.-P., Fritsch, E., Guyot, F., and Brown, G.E. (2009) XANES evidence for oxidation of Cr(III) to Cr(VI) by Mn-oxides in a lateritic regolith developed on serpentinized ultramafic rocks of New Caledonia. Environmental Science and Technology, 43, 7384–7390.

Fritsch, A., Dormieux, L., Hellmich, C., and Sanahuja, J. (2007) Micromechanics of crystal interfaces in polycrystalline solid phases of porous media: Fundamentals and application to strength of hydroxyapatite biomaterials. Journal of Materials Science, 42, 8824–8837.

Girard, L., Weiss, J., and Amitrano, D. (2012) Damage-cluster distributions and size effect on strength in compressive failure. Physical Review Letters, 108, 225502.

Grazulis, S., Chateigner, D., Downs, R.T., Yokochi, A.T., Quiros, M., Lutterotti, L., Manakova, E., Butkus, J., Moeck, P., and Le Bail, A. (2009) Crystallography Open Database—an open-access collection of crystal structures. Journal of Applied Crystallography, 42, 726–729.

Gurevich, B. (2003) Elastic properties of saturated porous rocks with aligned fractures. Journal of Applied Geophysics, 54, 203–218.

Hazemann, J.L., Berar, J.F., and Manceau, A. (1991) Rietveld studies of the aluminium-iron substitution in synthetic goethite. Materials Science Forum,

79, 821–826.
Hill, R. (1972) On constitutive macro-variables for heterogeneous solids at finite strain. Proceedings of the Royal Society A, 326, 131–147.
Hudson-Edwards, K.A., Schell, C., and Macklin, M.G. (1999) Mineralogy and geochemistry of alluvium contaminated by metal mining in the Rio Tinto area, southwest Spain. Applied Geochemistry, 14, 1015–1030.
Jackson, I. and Faul, U.H. (2010) Grainsize-sensitive viscoelastic relaxation in olivine: Towards a robust laboratory-based model for seismological application. Physics of the Earth and Planetary Interiors, 183, 151–163.
Jakobsen, M., Hudson, J.A., Minshull, T.A., and Singh, S.C. (2000) Elastic properties of hydrate-bearing sediments using effective medium theory. Journal of Geophysical Research—Solid Earth, 105, 561–577.
Kashef, S., Asgari, A., Hilditch, T.B., Yan, W., Goel, V.K., and Hodgson, P.D. (2011) Fatigue crack growth behavior of titanium foams for medical applications. Material Science and Engineering A, 528, 1602–1607.
Kawada, Y. and Yoshida, S. (2010) Formation of a hydrothermal reservoir due to anhydrite precipitation in an arc volcano hydrothermal system. Journal of Geophysical Research—Solid Earth, 115, B11106.
Levien, L., Prewitt, C.T., and Weidner, D.J. (1980) Structure and elastic properties of quartz at pressure. American Mineralogist, 65, 920–930.
Madsen, I.C. and Scarlett, N.V.Y. (2008) Quantitative phase analysis. In R.E. Dinnabier, Ed., Powder Diffraction: Theory and practice, 11, p. 298–331. Royal Society of Chemistry, London.
Mañosa, L., Planes, A., Rouby, D., Morin, M., Fleischmann, P., and Macqueron, J.L. (1989) Acoustic emission field during thermoelastic martensitic transformations. Applied Physics Letters, 54, 2574–2576.
Michel, J.C., Lopez-Pamies, O., Castaneda, P.P., and Triantafyllidis, N. (2007) Microscopic and macroscopic instabilities in finitely strained porous elastomers. Journal of Mechanics and Physics of Solids, 55, 900–938.
Muralidharan, V. and Hui, C-Y. (2004) Stability of nanoporous materials. Macromolecular Rapid Communications, 25, 1487–1490.
Oberti, R., Boiocchi, M., Smith, D., and Medenbach, O. (2007) Aluminotaramite, alumino-magnesiotaramite, and fluoro-alumino-magnesiotaramite: Mineral data and crystal chemistry. American Mineralogist, 92, 1428–1435.
Petri, A., Paparo, G., Vespignani, A., Alippi, A., and Constantini, M. (1994) Experimetnal-evicdence for critical-dynamics in microfracturing processes. Physical Review Letters, 73, 3423–3426.
Rathore, J.S., Fjaer, E., Holt, R.M., and Renlie, L. (1995) P-wave and S-wave anisotropy of a synthetic sandstone with controlled crack geometry. Geophysical Prospecting, 43, 711–728.
Rayner, J.H. and Brown, G. (1973) The crystal structure of talc. Clay and Clay Minerals, 21, 103–114.
Rodriguez-Navarro, C. and Sebastian, E. (1996) Role of particulate matter from vehicle exhaust on porous building stones (limestone) sulfation. Science of the Total Environment, 187, 79–91.
Rouby, D., Fleischmann, P., and Duvergier, C. (1983a) An acoustic-emission source model for both continuous and burst-type emission analysis. I.-Theory. Philosophical Magazine, A, 47, 671–687.
——— (1983b) An acoustic-emission source model for both continuous and burst-type emission analysis. II.-Experiments. Philosophical Magagazine, A, 47, 641–687.
Salje, E.K.H., Koppensteiner, J., Reinecker, M., Schranz, W., and Planes, A. (2009) Jerky elasticity: Avalanches and the martensitic transition in Cu74.08Al23.13Be2.79 shape-memory alloy. Applied Physics Letters, 95, 231908.
Salje, E.K.H., Zhang, H., Idrissi, H., Schryvers, D., Carpenter, M.A., Moya, X., and Planes, A. (2009) Mechanical resonance of the austenite/martensite interface and the pinning of the martensitic microstructures by dislocations in Cu74.08Al23.13Be2.79. Physical Review B, 80, 134114.
Salje, E.K.H., Koppensteiner, J., Schranz, W., and Fritsch, E. (2010) Elastic instabilities in dry, mesoporous minerals and their relevance to geological applications. Mineralogical Magazine, 74, 341–350.
Salje, E.K.H., Soto-Parra, D.E., Planes, A., Vives, E., Reinecker, M., and Schranz, W. (2011) Failure mechanism in porous materials under compression: crackling noise in mesoporous SiO_2. Philosophical Magazine Letters, 91, 554–560.
Scherer, G.W. (1998) Crystallization in pores. Cement and Concrete Research, 29, 1347–1358.
Schwertmann, U. and Latham, M. (1986) Properties of iron oxides in some New Caledonian oxisols. Geoderma, 39, 105–123.
Sethna J., Dahmen, K.A., and Perkovic, O. (2006) Random-field Ising models of hysteresis. In G. Bertotti and I. Mayergoyz, Eds., The Science of Hysteresis, vol. II, p. 107–179. Academic Press, San Diego.
Spieler, O., Kennedy, B., Kueppers, U., Dingwell, D.B., Scheu, B., and Taddeucci, J. (2004) The fragmentation threshold of pyroclastic rocks. Earth and Planetary Science Letters, 226, 139–148.
Tornos, F. (2006) Environment of formation and styles of volcanogenic massive sulfides: The Iberian Pyrite Belt. Ore Geology Reviews, 28, 259–305.
Traore, D., Beauvais, A., Chabaux, F., Peiffert, C., Parisot, J.C., Ambrosi, J.P., and Colin, F.D. (2008) Chemical and physical transfers in an ultramatic rock weathering profile: Part 1. Supergene dissolution of Pt-bearing chromite. American Mineralogist, 93, 22–30.
Vallely, A.S. and Gillham, J.K. (1997) Conversion-temperature-property relationships in thermosetting systems: Property hysteresis due to microcracking of an epoxy/amine thermoset-class fiber composite. Journal of Applied Polymer Science, 64, 39–53.
Whittaker, E.J.W. (1956) The structure of chrysotile. II. Clino-chrysotile. Acta Crystallographica, 9, 855–862.

Manuscript received August 8, 2012
Manuscript accepted October 24, 2012
Manuscript handled by Sergio Speziale